Nano LIFE
Vol. 2, No. 2 (2012) 1240003 (6 pages)

DOI: 10.1142/S1793984411000487

World Scientific
www.worldscientific.com

ELECTRONIC, MAGNETIC, AND MECHANICAL PROPERTIES OF LINE-DEFECT EMBEDDED GRAPHENE NANORIBBONS: A FIRST-PRINCIPLES STUDY

ZHAOYONG GUAN
Department of Chemical Physics
University of Science and Technology of China
Hefei, Anhui 230026, P. R. China
guanzy@mail.ustc.edu.cn

XIAOJUN WU
CAS Key Laboratory of Materials for Energy Conversion
Hefei National Laboratory for Physical Science at the Microscale
and Department of Material Science and Engineering
University of Science and Technology of China
Hefei, Anhui 230026, P. R. China
xjwu@ustc.edu.cn

QUNXIANG LI
Department of Chemical Physics and Hefei National Laboratory
for Physical Science at the Microscale
University of Science and Technology of China
Hefei, Anhui 230026, P. R. China
liqun@ustc.edu.cn

Received 15 February 2012
Accepted 6 March 2012
Published 11 May 2012

We use first-principles method to investigate the electronic, magnetic, and mechanical properties of graphene nanoribbons (GNRs) with extended line defect. Particular attention has been placed on zigzag GNR with 5-8-5 line defect and armchair GNR with 4-8 line defect. The results show that the band gaps of GNRs can be effectively tuned by line defect, which depend on both their widths and the position of defect. The line-defect embedded GNRs are either metals or semiconductor with markedly reduced band gap. The band-gap reduction is attributed to the defect-induced impurity states. In particular, the metallic line-defect embedded zigzag GNRs are ferromagnetic at ground state, while those semiconducting ones are antiferromagnetic. Upon the line-defect embedded armchair GNRs, the band gaps vary periodically with the increasing widths. Our results imply the potential applications of line-defect embedded GNRs at nanoscale electronics.

Keywords: Graphene nanoribbon; line defect; electronic structure; first-principles calculations.

1. Introduction

Graphene, a true two-dimensional (2D) planar material with single-atomic thickness, has attracted wide research attention for its unique physical properties, such as massless Dirac Fermion behavior, room-temperature quantum Hall effect, and high carrier mobility.[1–3] In particular, graphene nanoribbons (GNRs), the 1D counterpart of 2D graphene, present versatile electronic and magnetic properties suitable for the applications of electronics and spintronics at nanoscale.[4–15] For example, the band gaps of GNRs are no longer zero, which depend on both their widths and crystallographic orientations. The band gaps of GNRs with zigzag-type edges (ZGNRs) reduce monotonically with the increased widths, while those of GNRs with armchair-type edges (AGNRs) decrease in an oscillating behavior.[13] Moreover, ZGNRs show special edge states, which are coupled in antiferromagnetic (AFM) order at their ground states. Therefore, half-metallicity can be achieved in ZGNRs by applying a transverse electrical field or chemically functionalizing their edges, providing GNRs great potential in the spintronics applications.[14,15]

Recently, the extended line defect can be observed experimentally in graphene, which originates from the structural mismatch during the growth of graphene on a metal surface.[16–18] The extended line defect divides graphene into domains with different orientations and thus can affect the electronic, thermal and magnetic properties of 2D graphene.[19–24] Theoretically, it has been reported that the electronic transport behaviors of graphenes and GNRs vary markedly with the embedded line defects and they can act as filter to create a valley-polarized beam of electrons or holes.[19–23] Kou *et al.* predict a weak ferromagnetic ground state with spin-polarized electrons localized along the extended line defect embedded in graphene.[23] In addition, the magnetic moment of graphene with line defect can be tuned by applying in-plane strain.

Although wide research attention has been placed on 2D graphenes with extended line defects, there is no much report on the line-defect embedded GNRs. In this paper, we present a comprehensive study on the line-defect embedded GNRs by using the first-principles method. Our results show that the electronic, mechanical, and magnetic properties of GNRs can be effectively tuned by introducing line defects within the GNRs.

2. Models and Methods

The first-principles calculations are performed using VASP package.[25–27] The projector augmented wave method[28] and spin-polarized density functional theory (DFT) with the generalized-gradient approximation of the Perdew–Burke–Eruzerh (PBE)[29] functional are used. The plane-wave cut-off energy is set as 520 eV. The conjugate gradient method is employed to fully relax the axial lattices and atomic positions until the force on each atom is less than 0.01 eV/Å. To model the 1D GNRs with line defect, a supercell that is doubly repeated units of perfect GNRs along the ribbon's direction is used. Two adjacent GNRs are separated by a vacuum region of 15 Å, and the 1D Brillouin zone is sampled by 40 special k-points.

3. Results and Discussions

The GNRs with line defect can be obtained by inserting a C_2 dimer per supercell into the lattice of a perfect GNR along the ribbon's direction, as shown in Fig. 1.[16] In ZGNRs, the inserted C_2 dimers lead to an extended line defect containing octagons and pentagons (5-8-5 line defect). In AGNRs, the inserted C_2 dimers lead to an extended line-defect including quadrangles and octagons (4-8 line defect). Here, we use n-LD-m GNR to label the GNRs with line defect, where n and m are integers and represent the widths of two ribbon domains separated by the line defect. For example, in Fig. 1,

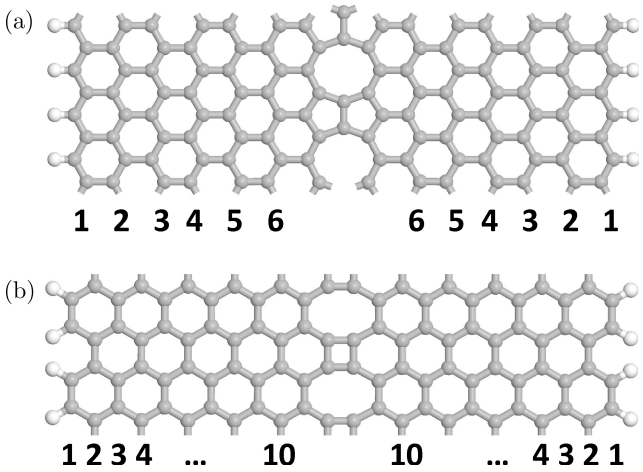

Fig. 1. The optimized structures of (a) 6-LD-6 ZGNR and (b) 10-LD-10 AGNR. The grey and white balls represent carbon and hydrogen atoms, respectively.

two GNRs with line defect are displayed, namely 6-LD-6 ZGNR and 10-LD-10 AGNR. The 6-LD-6 ZGNR here denotes that a ZGNR contains a 5-8-5 line defect, where each perfect ZGNR domain contains six zigzag carbon chains in the ribbon direction. Similarly, the 10-LD-10 AGNR represents an AGNR contains a 4-8 line defect, where each perfect AGNR domain contains 10 carbon chains in the ribbon direction.

At first, we investigate the electronic properties of perfect ZGNRs and AGNRs. In Fig. 2, the electronic band structures of 22-ZGNRs and 19-AGNRs, as well as the band gap of GNRs with various widths are presented. Here the numbers 22 and 19 represent the width of GNRs, using the same definition as that in line-defect embedded GNRs. Consistent with previous reports,[30–32] GNRs are semiconducting with direct and width-dependent band gaps. The band gap of ZGNR slightly decreases with increasing the widths, while that of AGNRs varies periodically with their increased widths. At their ground states, ZGNRs are AFM, while AGNRs are nonmagnetic (NM).

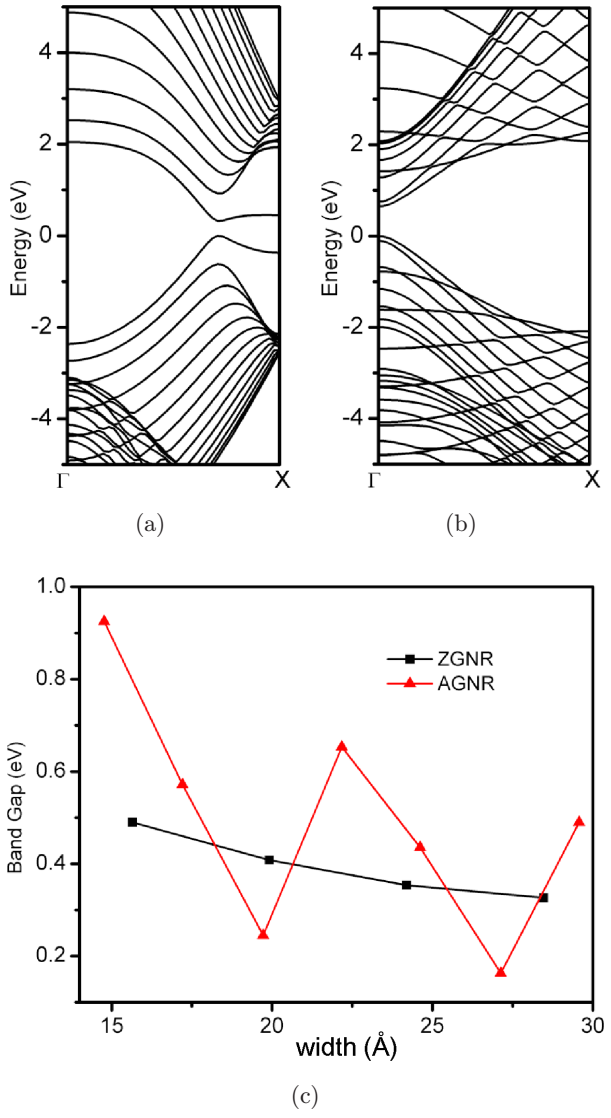

Fig. 2. The electronic band structures of GNRs. (a) 21-ZGNR, (b) 19-AGNR. Here, the Fermi level is set as zero for clarity. (c) The band gaps of GNRs with different widths.

3.1. *Electronic structures of ZGNR with line defect*

In Fig. 3, the electronic band structure and density of states (DOS) of 6-LD-6 ZGNR at the ground state are plotted. The 6-LD-6 ZGNR is a semiconductor with an indirect band gap of about 0.11 eV, which is smaller than that of perfect ZGNR with similar width (0.32 eV direct band gap at same calculation level). Clearly, the extended line defect induces impurity states around the Fermi level, which leads to the band-gap reduction, as shown in Fig. 2(b). The 6-LD-6 ZGNR is AFM at ground state. Similar with the perfect ZGNRs, the spin charge density in 6-LD-6 ZGNR mainly distributes over the edged carbon atoms. However, the energy difference between AFM and ferromagnetic (FM) states of 6-LD-6 ZGNR is about 7 meV, suggesting that the 6-LD-6 ZGNR presents paramagnetic behavior at low temperature.

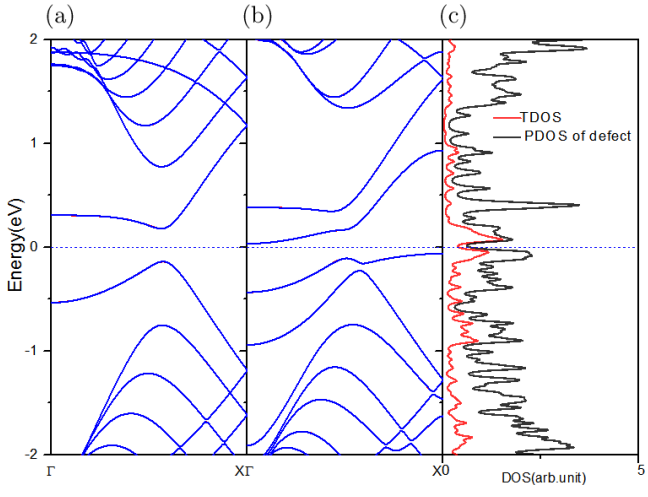

Fig. 3. (a) Band structures of perfect ZGNR. (b) Band structure and (c) DOS of the 6-LD-6 ZGNR. The Fermi level was set as zero. The black and red lines stand for the total DOS and DOS projected on the extended line-defect, respectively (color online).

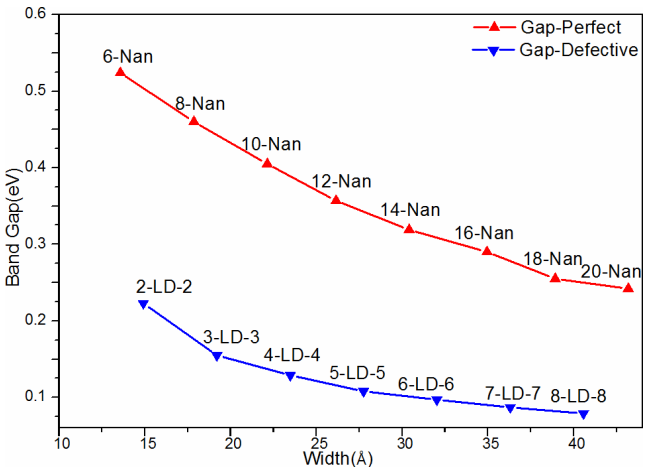

Fig. 4. The band gaps of perfect ZGNRs and 5-8-5 line-defect embedded ZGNRs are plotted for ribbons' widths.

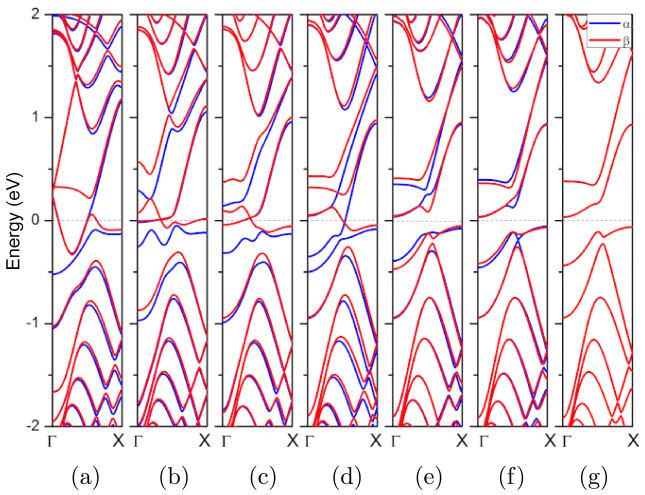

Fig. 5. The band structures of line-defect embedded ZGNRs. (a) 0-LD-12, (b) 1-LD-11, (c) 2-LD-10, (d) 3-LD-9, (e) 4-LD-8, (f) 5-LD-7, (g) 6-LD-6. Here, the Fermi level is set as zero for clarity, the red and blue lines represent the spin-up (α) and spin-down (β) states, respectively (color online).

Like perfect GNRs, the electronic band structures of ZGNRs with 5-8-5 line defect show the width-dependent band gap. The band gaps of n-LD-n ZGNRs are plotted for different values of n in Fig. 4. All n-LD-n ZGNRs are semiconductors with AFM ground state. In particular, the band gaps of n-LD-n are smaller than those of perfect ZGNRs with similar widths, which reduce monotonically with increasing widths. Note that GGA method always underestimates the band gap of semiconductors, the above conclusion, however, is still right.

Moreover, the electronic properties of n-LD-m ZGNRs are also sensitive to the position of line-defect within the ribbon. Compared with the semiconducting n-LD-n ZGNRs, the n-LD-m ZGNRs may be either semiconductors or metals depending on the values of n and m. For example, in Fig. 5, the electronic band structures of n-LD-m ZGNRs with $n + m = 12$ are plotted. As the line defect moves close to the edge (n decreases from 6 to 0), the n-LD-m ZGNR transfers from semiconductor to metal. As summarized in Table 1, the n-LD-m ZGNRs with line defect locating near the edge is energetically favorable. In addition, the metallic n-LD-m ZGNRs have FM ground states, while the semiconducting n-LD-m ZGNRs have AFM ground states. Similar theoretical results have been reported recently.[24] We also perform test calculations on the line-defect embedded ZGNRs with $n + m = 8$ and obtain same results.

3.2. *Electronic structures of AGNR with line defect*

The AGNR with 4-8 line defect can be obtained by inserting C_2 dimers into perfect AGNR. For example, Fig. 1(b) illustrates the 10-LD-10 AGNR, which is obtained by inserting C_2 dimer into a perfect 23-AGNR. The band structure and DOS of 10-LD-10 AGNR are plotted in Fig. 6(b) and 6(c). As a comparison, the band structure of perfect 23-AGNR is plotted in Fig. 6(a). The band gap of 10-LD-10 AGNR is about 0.33 eV, which is smaller than that of 23-AGNR (about 0.50 eV at same calculation level). This is partly due to the impurity states induced by the line-defect. The AGNRs with line defect have NM ground states.

Table 1. The total energy (E) per supercell, magnetic moment (M) per supercell and band gap (gap) of n-LD-m ZGNRs.

	E (eV)	M (μ_B)	Gap (eV)
0-LD-12	−545.496	0.35	0.000
1-LD-11	−545.226	0.54	0.000
2-LD-10	−545.079	0.21	0.000
3-LD-9	−545.138	0.54	0.000
4-LD-8	−545.112	0.00	0.103
5-LD-7	−545.129	0.00	0.097
6-LD-6	−545.107	0.00	0.110

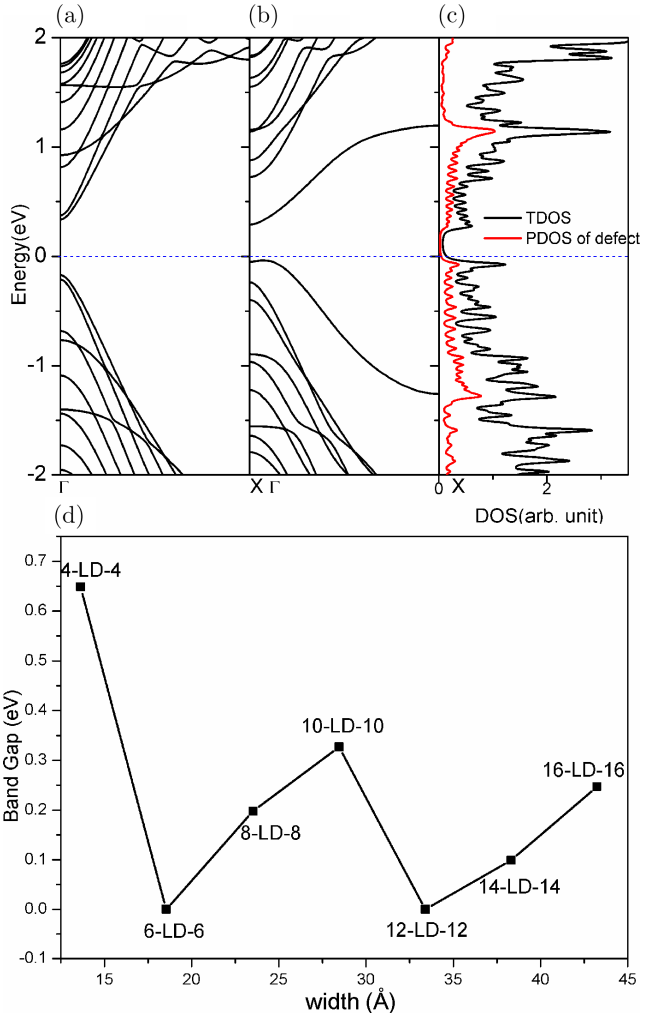

Fig. 6. (a) Band structure of perfect 23-AGNR. (b) Band structure and (c) DOS of 10-LD-10 AGNR. Here, the Fermi level is set as zero, and the TDOS and DOS projected on the line defect are plotted with black and red lines, respectively. (d) The band gap of n-LD-n AGNRs are plotted with various widths (color online).

Similar with the line-defect embedded ZGNRs, the band gaps of line-defect embedded AGNRs also depend on both their widths and the position of defect. As shown in Fig. 6(d), the band gaps of n-LD-n vary periodically with increasing width, similar to that of perfect AGNRs [Fig. 2(c)], as well as the band gaps are smaller than those of the perfect AGNRs with similar widths. In addition, the band gaps of AGNRs vary markedly with the position of line defect within the nanoribbons. As shown in Fig. 7, the bang gaps of n-LD-m AGNRs are plotted with various n and m. Similarly, n-LD-m AGNRs may be either metallic or semiconducting dependent on their widths and position of line

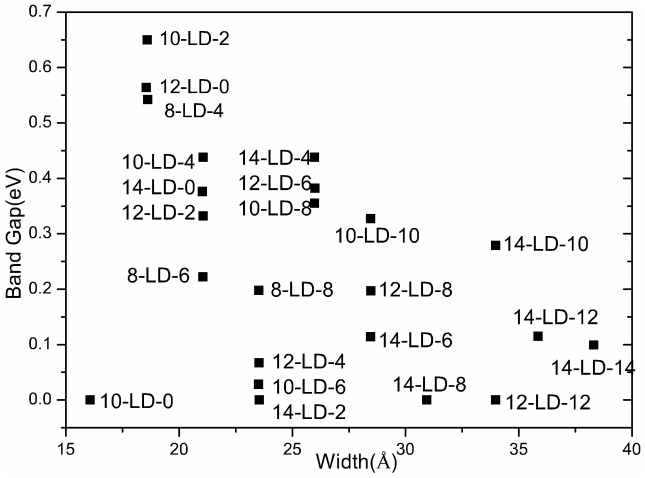

Fig. 7. The band gaps of n-LD-m AGNRs with different n and m values.

defect. However, both metallic and semiconducting n-LD-m ANGRs have NM ground states.

3.3. *Mechanical properties of GNRs with line defect*

Finally, the elastic properties of GNRs with line defect are investigated. Similar to the previous study,[33] the Young's modulus (Y) of 1D GNR can be defined as $Y = (\partial^2 E/\partial\varepsilon^2)/V_0$, where E is the total energy of GNR per supercell. V_0 is the relaxed volume of GNR per unit cell without uniaxial strain, defined as $V_0 = w \times h_0 \times c_0$, where w is the width, h_0 is the thickness, and c_0 is the periodic length along the ribbon direction of GNR. Here the interlayer distance of graphite is chosen as the thickness of GNR, where h_0 is set as 3.35 Å; ε is the axial strain, which is defined as $(c - c_0)/c_0$.

To assess the effect of line defect on the mechanical properties of GNRs, we take 4-LD-4 ZGNR with the width of about 23.47 Å as an example. The calculated Young's modulus is about 923 GPa, which is reduced by about 10% compared with 1030 GPa of the pristine 10-ZGNR (21.90 Å). Thus, the line-defect will slightly reduce the Young's modulus of ZGNR. Moreover, the position of line-defect also affects the Young's modulus of ZGNR. The Young's modulus of 0-LD-8, 1-LD-7, 2-LD-6, are 1005, 957, 926 GPa, respectively, suggesting the Young's modulus of line-defect embedded ZGNRs increases slightly when the defect moves close to the edge. Similar results have been confirmed on the line-defect embedded ZGNRs with various widths and AGNRs.

4. Conclusion

In conclusion, we investigate the electronic, magnetic and mechanical properties of ZGNRs with 5-8-5 line defect and AGNRs with 4-8 line defect by using first-principles method. Our results show that the electronic and magnetic properties of GNRs can be effectively tuned by introducing extended line defect. The line-defect embedded GNRs may be either metallic or semiconducting with a reduced band gap depending on both their widths and the distribution of line defect. The band gap of n-LD-n ZGNRs reduces monotonically with the increasing width, while that of n-LD-n AGNRs varies periodically. At ground state, the semiconducting line-defect embedded ZGNRs are AFM, while those metallic line-defect embedded ZGNRs are FM. The existence of line defect slightly lower the Young's modulus of GNRs and the Young's modulus of line-defect GNRs also depends on the position of line defect.

Acknowledgments

This work was partially supported by NKBRPC (Grant No. 2011CB921400, 2012CB922001), NSFC (Grant No. 21121003, 11004180, 51172223, 91021004, 11074235, 11034006), by the Fundamental Research Funds for Central Universities (No. WK2340000007), by One Hundred Person Project of CAS, by Shanghai Supercomputer Center and Supercomputing Center of USTC.

References

1. K. S. Novoselov, A. K. Geim, S. V. Morozov, D. Jiang, M. I. Katsnelson, I. V. Grigorieva, S. V. Dubonos and A. A. Firsov, *Nature* **438**, 197 (2005).
2. Y. Zhang, Y.-W. Tan, H. L. Stormer and P. Kim, *Nature* **438**, 201 (2005).
3. C. Berger, Z. Song, X. Li, X. Wu, N. Brown, C. Naud, D. Mayou, T. Li, J. Hass, A. N. Marchenkov, E. H. Conrad, P. N. First and W. A. de Heer, *Science* **312**, 1191 (2006).
4. M. Y. Han, B. Özyilmaz, Y. Zhang and P. Kim, *Phys. Rev. Lett.* **98**, 206805 (2007).
5. Z. Chen, Y.-M. Lin, M. J. Rooks and P. Avouris, *Physica E* **40**, 228 (2007).
6. X. Li, X. Wang, L. Zhang, S. Lee and H. Dai, *Science* **319**, 1229 (2008).
7. K. Wakabayashi, M. Fujita, H. Ajiki and M. Sigrist, *Phys. Rev. B* **59**, 8271 (1999).
8. M. Fujita, K. Wakabayashi, K. Nakada and K. Kusakabe, *J. Phys. Soc. Japan* **65**, 1920 (1996).
9. Y. Miyamoto, K. Nakada and M. Fujita, *Phys. Rev. B* **59**, 9858 (1999).
10. Y.-W. Son, M. L. Cohen and S. G. Louie, *Nature* **444**, 347 (2006).
11. S. Okada and A. Oshiyama, *Phys. Rev. Lett.* **87**, 146803 (2001).
12. H. Lee, Y.-W. Son, N. Park, S. Han and J. Yu, *Phys. Rev. B* **72**, 174431 (2005).
13. L. Yang, C.-H. Park, Y.-W. Son, M. L. Cohen and S. G. Louie, *Phys. Rev. Lett.* **99**, 186801 (2007).
14. Y. W. Son, M. L. Cohen and S. Louie, *Nature* **8**, 241 (2008).
15. E. J. Kan, Z. Y. Li, J. L. Yang and J. G. Hou, *J. Am. Chem. Soc.* **130**, 4224 (2008).
16. J. Lahiri, Y. Lin, P. Bozkurt, I. I. Oleynik and M. Batzill, *Nature Nanotech* **5**, 326 (2010).
17. J. Coraux, A. T. N'Diaye, C. Busse and T. Michely, *Nano Lett.* **8**, 565 (2008).
18. J. Cervenka, M. I. Katsnelson and C. F. J. Flipse, *Nature Phys.* **5**, 840 (2009).
19. O. V. Yazyev and S. G. Louie, *Nature Mat.* **9**, 806 (2010).
20. F. Banhart, J. Kotakoshi and A. V. Krasheninnikov, *ACS Nano* **5**, 26 (2011).
21. B. W. Jeong, J. Ihm and G. D. Lee, *Phys. Rev. B* **78**, 165403 (2008).
22. D. Gunlycke and C. T. White, *Phys. Rev. Lett.* **106**, 136806 (2011).
23. L. Kou, C. Tang, W. Guo and C. Chen, *ACS Nano* **5**, 1012 (2011).
24. X. Q. Li and J. Ni, *Phys. Rev. B* **84**, 075461 (2011).
25. G. Kresse and J. Hafner, *Phys. Rev. B* **47**, 558 (1993).
26. G. Kresse and J. Hafner, *Phys. Rev. B* **49**, 14251 (1994).
27. G. Kresse and J. Furthmüller, *Phys. Rev. B* **54**, 11169 (1996).
28. G. Kresse and D. Joubert, *Phys. Rev. B* **59**, 1758 (1999).
29. J. P. Perdew, K. Burke and M. Ernzerhof, *Phys. Rev. Lett.* **77**, 3865 (1996).
30. K. Nakada and M. Fujita, *Phys. Rev. B* **54**, 17954 (1996).
31. Y. Miyamoto, K. Nakada and F. Mitsutaka, *Phys. Rev. B* **59**, 9858 (1999).
32. Y. W. Son, M. L. Cohen and S. G. Louie, *Phys. Rev. Lett.* **97**, 216803 (2006).
33. X. J. Wu, Z. P. Xu and X. C. Zeng, *Nano Lett.* **7**, 2987 (2007).